Chapter Two

## Single Kink Dynamics in an Easy-Plane Ferromagnet

### 2.1 Easy-plane Ferromagnets

We would like to investigate the classical spin dynamics for a model of a one-dimensional magnet. The physical systems under consideration consist of chains of spins, with strong ferromagnetic exchange J between nearest neighbor spins on a chain, and much weaker second nearest neighbor interactions. Interactions of spins on different chains can be entirely ignored, since they are typically a factor of $10^3$ smaller. There is also a single ion anisotropy field A which makes one spin direction (for instance, $\hat{z}$) higher energy than the other two. Then the plane whose normal is parallel to this anisotropy field is referred to as an easy plane, since the spins will preferably lie in that plane to minimize their energy. If we also include an applied magnetic field $\vec{B}$ in the easy plane, then the ground state of the spins is uniquely determined, being the configuration with all spins aligned with the field. With the xy plane as this easy plane, and applied field in the x-direction (in spin space), a model Hamiltonian for these materials is

$$H = \sum_n \left(-J\vec{S}_n \cdot \vec{S}_{n+1} + A(S_n^z)^2 - g\mu_B B_x S_n^x\right) \quad . \tag{2-1}$$

The sum is over all lattice sites, $\vec{S}_n$ is the classical spin vector at site n, and J, A and $B_x$ are all positive parameters. g and $\mu_B$ are the Landé g-factor and Bohr magneton respectively, and are necessary if we take $B_x$ to have dimensions of magnetic field. J and A have dimensions of energy (or temperature), and the spin vectors are dimensionless.

One of the better known real materials for which this model Hamiltonian is believe to be applicable is the spin-1 magnet $CsNiF_3$. The

structure of $CsNiF_3$ has been determined through quasi-elastic neutron scattering by Babel (1969). The compound crystallizes in the hexagonal space group $P6_3/mmc$, with two formula units per unit cell. The unit cell parameters are a = b = 6.21 Å, c = 5.20 Å. Each $Ni^{2+}$ ion is surrounded by six $F^-$ ions, located at the vertices of a slightly distorted octahedron. These $F^-$ ions form "cages" for the chains of $Ni^{2+}$ ions, and are responsible for the intrachain superexchange. The Ni-Ni distance along the chains is 2.6 Å, which from chain to chain it is 6.2 Å. This plus the fact that the interchain superexchange path is through two $F^-$ ions causes the interchain exchange to be negligible compared to the intrachain exchange. The compound can be expected to have 1-D properties simply on the basis of the structure. Quasi-elastic neutron scattering (Steiner and Dachs 1971) has shown that J = 23.6 K.

The electron configuration of $Ni^{2+}$ is $[Ar]3d^8$; the two holes in the d-orbital are responsible for the magnetic properties. A theoretical treatment of the crystal field of the $F^-$ ions on the $Ni^{2+}$ wavefunction through perturbation theory shows that the energy of the molecule should have an easy-plane anisotropy with respect to the spin direction (Hutchings 1964). From the experimental viewpoint, it has been shown that results of magnetic susceptibility measurements depend on whether one has $\vec{B}\|\hat{c}$ or $\vec{B}\|\hat{a},\hat{b}$ (Steiner et al. 1971). Thus it has been shown that the ab plane is an easy plane. Also, susceptibility measurements have provided further evidence for the one-dimensionality. At temperatures below 80 K, there are deviations in $\chi$ from that predicted by the Curie-Weiss law, indicative of 1-D ordering. From 20 K to 4.2 K there is no evidence of interchain interactions (Steiner and Dachs 1971). However, at $T_N$ = 2.65 K, there is a phase transition to a 3-D antiferromagnet, indicating that the interchain exchange J' is less than 1/200 of the

intrachain exchange J. This estimate comes from Oguchi's (1964) relation between the 3-D transition temperature $T_N$ and $|J'/J|$. The transition to a 3-D compound is also indicated by a peak in the specific heat at T = 2.613 K, as found by Lebesque et al. (1973). They also made high temperature susceptibility measurements on powder samples to estimate $\bar{g}$ (averaged over all directions); these have been refined to give only the in-plane component of g = 2.4 (Steiner 1981, Steiner et al. 1983).

Inelastic neutron scattering by spin waves in the presence of an applied field (Steiner and Kjems 1977) has shown that the anisotropy constant A = 9.0 K for the quantum Hamiltonian, and A = 4.5 K must be used for the classical Hamiltonian. There is a renormalization of A in going from the spin-1 quantum case to the classical case, exactly by a factor of ½. The parameter A can also be obtained from susceptibility measurements (Dupas and Renard 1975, Lebesque and Huyboom 1976, and Montano 1977).

A more recently discovered spin-½ magnet is $(C_6H_{11}NH_3)CuBr_3$, cyclohexylammonium tribromocuprate, or "CHAB". This compound is believed to be isomorphic to the better studied ferromagnet $(C_6H_{11}NH_3)CuCl_3$, or CHAC, whose structure has been determined (Groenendijk et al. 1981). The CHAC crystal is orthorhombic, space group $P2_12_12_1$(z = 4), with a = 19.441 Å, b = 8.549 Å and c = 6.190 Å, and two formula units per unit cell. The compound has bibridged linear chains of $CuCl_3^-$ ions parallel to $\hat{c}$. These chains are hydrogen bonded together in the b-c plane by the $NH_3^+$ moiety. The Cu-Cu distance is 3.138 Å intrachain, and approximately 8.5 Å interchain. One expects slightly different structural parameters for the bromine compound due to the larger size of Br compared to Cl.

Specific heat measurements by Kopinga et al. (1982) on both compounds have shown that CHAB is an easy-plane ferromagnet with 5% anisotropy, and

$J_x = J_y = 110$ K ($J_z = 0.95\ J_x$), while CHAC is an easy-axis ferromagnet with 2% anisotropy and $J_z = 45$ K ($J_x = J_y = 0.98\ J_z$). Note that one really must use exchange anisotropy (rather than a single ion term) for a spin-½ quantum Hamiltonian. In the classical dynamics for CHAB under consideration here we will take J = 110 K and A = 5.5 K. Finally, it has also been determined that CHAB undergoes a transition to 3-D order at $T_N = 1.5$ K, and the interchain coupling $J' \lesssim 10^{-3}J$ and we shall take g = 2.0 (Kopinga et al. 1982, 1984).

## 2.2 Spin Dynamics

This model is believed to describe the low temperature thermodynamics of these linear chain ferromagnets, such as $CsNiF_3$ and CHAB, at temperature greater than their 3-D ordering temperature $T_N$. We will not directly investigate the classical thermodynamics, since this has been done by others (see for example Leung and Bishop 1983, Osano 1984). Rather, we are interested in analyzing the dynamic excitations of the model, especially the nonlinear localized soliton-like excitations that generally will be referred to as "kinks". We prefer to reserve the term "soliton" for localized excitations that behave as independent particles and preserve their waveform asymptotically after collisions (i.e. solitary traveling waves). In the limit of large anisotropy field A compared to J, the spins are strongly restricted to motions only in the easy plane. In the limit of small applied field $B_x$ relative to J, effects of having spins on a discrete lattice will be shown to be unimportant, and the continuum limit is justified. With the combination of large anisotropy and small applied field, the dynamics for the angle $\phi$ of the spins measured from the x-axis in the easy plane is well described by the sine-Gordon (sG) equation (Mikeska 1978),

$$\phi_{\xi\xi} - \phi_{\tau\tau} = b \sin \phi \quad b \equiv g\mu_B B_x/2AS \tag{2-2}$$

This is obtained using appropriate space and time units below.

Equation (2-2) is known to be completely integrable, and have for its solutions solitons and antisolitons, breathers (bound soliton-anti-soliton pairs) and small amplitude traveling waves, or spin waves in the present context (Ablowitz et al. 1973, Takhtadzhyan and Faddeev 1974). For a review of solitons and their properties see Bishop et al. (1980) and Scott et al. (1973). A soliton or antisoliton is a rotation of $\phi$ through $2\pi$ radians over a characteristic width $2(JS/g\mu_B B_x)^{1/2}$, with the spins exactly confined to the easy plane if the soliton is stationary. Generally the soliton is a traveling-wave pulse, whose width depends on the velocity. In this sG limit of the equations of motion, the out-of-plane angle $\theta$, which measures the tipping of the spins out of the easy plane, is proportional to the time derivative of the in-plane angle $\phi$. This extra degree of freedom generally destroys the solitary wave character of these excitations, hence they will be called kinks. Also, if the applied field is large compared to the anisotropy field, then it can be energetically favorable for the spins to tip out of the easy plane instead of pointing against the magnetic field. The combined effects of velocity and large applied field can cause the sG kink to become unstable (Kumar 1982, Magyari and Thomas 1982), acquiring large-out-of-plane angle $\theta$, in which case the original assumption of $\theta \ll 1$ breaks down. Then the sG limit of the equations of motion is no longer valid, and one must use the original equations of motion without making this assumption. This kink instability is one topic we would like to investigate. Also, there is the task of determining what nonlinear excitation replaces the sG kink when the sG assumptions do not apply.

Since it is difficult to exactly solve the full nonlinear equations of motion for arbitrary A, J and $B_x$, we will resort to numerical simulations. There are two types of numerical experiments we have performed. Both involve integrating the discrete equations of motion for $\phi_n$ and $\theta_n$, the in-plane and out-of-plane angles at lattice site n. The first experiment involves starting with a sG kink profile as the initial conditions, discretized for the lattice, and then following the resulting time evolution. The kink position and velocity can then be measured as a function of time, and an average velocity v is obtained. We then can compare the results, especially the dispersion relation E(v), where E is the energy, with preditions of the pure sG theory. Generally one finds strong deviations from the sG theory, due to large out-of-plane motions. The second experiment starts with a kink-anti kink profile, and follows the time evolution during a collision of the two. A variety of outcomes are possible, as a function of A and $B_x$ with J fixed. The three major outcomes are transmission of the kinks, formation of a kink-antikink bound or oscillatory state, or a reflection of the kink-antikink pair. Details of both experiments are given below.

There is another approach to obtain dynamical information - the use of various Ansätze for kink traveling wave profiles. Some of these are motivated from the linear stability analysis, which will be described here. There is an Ansatz in terms of the xyz spin components by Liebmann et al. (1983), which closely reproduces results of these numerical simulations, and we use it later as partial motivation for a kink Ansatz in a similar antiferromagnetic chain (Chapter 6). In all of these calculations a two-parameter profile for the kink is assumed, and the parameters are determined by extremizing the Lagrangian with respect to variations in them. More properly, an action principle should be used, that is, the

time integral of the Lagrangian should be extremized, but for these traveling wave profiles the Lagrangian is a constant in time, so that this is not necessary.

## 2.3 Sine Gordon Kinks

The dynamical equations resulting from Eq. (2-1) can be obtained via Poisson brackets as

$$\dot{\vec{S}}_n = \{\vec{S}_n, H\} = \vec{S}_n \times \vec{F}_n \tag{2-3a}$$

$$\vec{F}_n = J(\vec{S}_{n-1} + \vec{S}_{n+1}) + g\mu_B \vec{B} - 2AS_n^z \hat{z} \quad . \tag{2-3b}$$

Here $\hat{z}$ is the unit vector in the z direction, $\vec{S}_n \times \vec{F}_n$ is the torque on the spin at site n. If the spin variables are written in terms of spherical polar coordinates as

$$\vec{S}_n = S(\cos\theta_n \cos\phi_n, \cos\theta_n \sin\phi_n, \sin\theta_n) \quad , \tag{2-4}$$

then the discrete equations of motion for $\theta_n$ and $\phi_n$ are

$$\begin{aligned}(\hbar/JS)\dot{\phi}_n \cos\theta_n = {} & \sin\theta_n[\cos\theta_{n+1}\cos(\phi_{n+1}-\phi_n) + \cos\theta_{n-1}\cos(\phi_{n-1}-\phi_n)] \\ & - \cos\theta_n(\sin\theta_{n+1} + \sin\theta_{n-1}) + (2A/J)\cos\theta_n \sin\theta_n \\ & + (g\mu_B B_x/JS)\sin\theta_n \cos\phi_n \end{aligned} \tag{2-5a}$$

$$\begin{aligned}(\hbar/JS)\dot{\theta}_n = {} & \cos\theta_{n+1}\sin(\phi_{n+1}-\phi_n) + \cos\theta_{n-1}\sin(\phi_{n-1}-\phi_n) \\ & - (g\mu_B B_x/JS)\sin\phi_n \quad . \end{aligned} \tag{2-5b}$$

For these equations, if we were to use time units $(\hbar/JS)$, then it is seen that the two parameters $\alpha \equiv 2A/J$ and $\beta \equiv g\mu_B B_x/JS$ determine the nature of

the time evolution for a given initial condition. In order to obtain the continuum limit the discrete index n is replaced by position z, and we assume slow spatial variations in $\theta$ and $\phi$, which go over into continuous fields $\theta_n \to \theta(z,t)$, $\phi_n \to \phi(x,t)$. Using the usual Taylor series expansions for $\theta_{n-1}$, $\theta_{n+1}$ and so on, we obtain the partial differential equations (Magyari and Thomas 1982)

$$\phi_\tau \cos\theta = -\theta_{\xi\xi} + (1-\phi_\xi^2)\sin\theta\cos\theta + b\,\sin\theta\cos\phi \quad , \tag{2-6a}$$

$$\theta_\tau = \phi_{\xi\xi}\cos\theta - 2\theta_\xi\phi_\xi\sin\theta - b\,\sin\phi \quad , \tag{2-6b}$$

$$b \equiv \beta/\alpha = g\mu_B B_x/2AS \quad . \tag{2-6c}$$

The space and time units here are $\xi^2 = (2A/Ja^2)z^2$ and $\tau = (2AS/\hbar)t$, where a is the lattice spacing. Subscripts denote partial derivatives. We now see that only one constant, b is necessary to specify the time evolution resulting from a given initial profile. The effects of discreteness of the lattice have been removed.

To obtain the sine-Gordon limit (Mikeska 1978), it is assumed that $\theta$, $b \ll 1$, and considering $\partial/\partial\xi$, $\partial/\partial\tau$, $\theta$ and b all to be of comparable order of smallness, the leading terms in (2-6) are

$$\phi_\tau = \theta \tag{2-7a}$$

$$\theta_\tau = \phi_{\xi\xi} - b\,\sin\phi \quad . \tag{2-7b}$$

$\theta_\tau$ can be eliminated from (2-7b) to give the sine-Gordon equation for $\phi$:

$$\phi_{\xi\xi} - \phi_{\tau\tau} = b\,\sin\phi \quad . \tag{2-8}$$

With boundary conditions $\phi(z = -\infty) = 0$, $\phi(z = +\infty) = 2\pi$, the single kink solution, moving with velocity u, is easily verified to be

$$\phi_{sG} = 4 \tan^{-1} \exp[\gamma b^{1/2}(\xi - u\tau)] \tag{2-9a}$$

with

$$\gamma \equiv (1-u^2)^{-1/2} \tag{2.9b}$$

The characteristic static kink width in these units is $b^{-1/2}$, and converted back to lattice units is $b^{-1/2}\alpha^{-1/2}a = (JS/g\mu_B B_x)^{1/2}a = \beta^{-1/2}a$. Therefore we see that we need the length scale ratio $\beta^{-1/2} \gg 1$ if we are to obtain smooth sG kinks. From this in-plane profile, the out-of-plane profile is

$$\theta_{sG} = -2\gamma b^{1/2} u \operatorname{sech}[\gamma b^{1/2}(\xi - u\tau)] \quad . \tag{2-10}$$

The amplitude of this $\theta$ profile is therefore directly proportional to the kink velocity. For the sine-Gordon limit to be valid, one then must require $2\gamma b^{1/2} u \ll 1$. But this turns out not to be the only requirement. To investigate further what is needed, we will turn to a linear stability analysis. But first, the kink energy will be determined.

The continuum limit Hamiltonian has been shown to be

$$H = \varepsilon_0 \int d\xi \{\frac{1}{2}(\frac{\partial \hat{\sigma}}{\partial \xi})^2 + \frac{1}{2}(\hat{\sigma}^z)^2 + b(1-\sigma^x)\}$$

$$= \varepsilon_0 \int d\xi \{\frac{1}{2}(\theta_\xi^2 + \phi_\xi^2 \cos^2\theta) + \frac{1}{2}\sin^2\theta + b(1 - \cos\theta\cos\phi)\} \tag{2-11a}$$

where

$$\varepsilon_0 = (2AJ)^{1/2} S^2 \tag{2-11b}$$

and $\hat{\sigma}$ is a unit vector spin variable ($\vec{S} = S\hat{\sigma}$). A constant has been added to H to make the ground state energy zero. The energy $E_{sG}$ of the sG kink is then

$$E_{sG} = 8\varepsilon_0 b^{1/2}\gamma \quad . \tag{2-12}$$

The kink has a rest (or creation) energy $8\varepsilon_0 b^{1/2}$, and its energy increases monotonically with velocity by the relativistic factor $\gamma$.

## 2.4 Static sG Kink Linear Stability Analysis

In order to test the stability of the static sG kink (Kumar 1982a, Magyari and Thomas 1982) we assume a perturbation from the static sG kink solution, and substitute back into the original continuum equations of motion (2-6). Only for $u = 0$ is solution (2-9), (2-10) exact for (2-6), so this is why the static kink stability is simplest to determine analytically. Take

$$\phi = \phi_{sG} + \tilde{\phi} \tag{2-13a}$$

$$\theta = \theta_{sG} + \tilde{\theta} \tag{2-13b}$$

where $\tilde{\theta}$, $\tilde{\phi} \ll 1$. That is, linearize equations (2-6) with respect to $\tilde{\theta}$ and $\tilde{\phi}$, and obtain the following equations:

$$\tilde{\phi}_\tau = -\tilde{\theta}_{\xi\xi} + (1 - \phi^2_{sG\xi} + b\cos\phi_{sG})\tilde{\theta} \tag{2-14a}$$

$$\tilde{\theta}_\tau = \tilde{\phi}_{\xi\xi} - b\cos\phi_{sG} \quad . \tag{2-14b}$$

On, after inserting the known solution for $\phi_{sG}$, we have

$$\dot{\tilde{\phi}} = -\tilde{\theta}_{xx} + (1 + 1/b - 6\,\mathrm{sech}^2 x)\tilde{\theta} \tag{2-15a}$$

$$\dot{\tilde{\theta}} = \tilde{\phi}_{xx} - (1 - 2\,\mathrm{sech}^2 x)\tilde{\phi} \tag{2-15b}$$

where $x = \beta^{1/2} z$, and dot implies $(1/g\mu_B B_x)\partial/\partial t$. An exact complete set of solutions for these equations is not known. If there exists a solution, however, which grows with time, then the original static sG kink is unstable towards that mode. Another way to look at the stability is to expand the Hamiltonian to leading (quadratic) order in $\tilde{\theta}$ and $\tilde{\phi}$ (Kumar 1982a); doing so obtains

$$H = E_{sG}(u=0) + \frac{b}{2}\varepsilon_0 \int d\xi \; f(\tilde{\theta},\tilde{\phi}) \tag{2-16a}$$

$$f(\tilde{\theta},\tilde{\phi}) = (1 + 1/b - 6\,\mathrm{sech}^2 x)\tilde{\theta}^2 + \tilde{\theta}_x^2 - (4\,\mathrm{sech}\, x \tanh x)\tilde{\phi}$$

$$+ (1 - 2\,\mathrm{sech}^2 x)\tilde{\phi}^2 + (4\,\mathrm{sech}\, x)\tilde{\phi}_x + \tilde{\phi}_x^2 \quad . \tag{2-16b}$$

The function f is rewritten in terms of normal modes

$$\int dx \; f(\tilde{\theta},\tilde{\phi}) = \int dx(\lambda_\theta \tilde{\theta}^2 + \lambda_\phi \tilde{\phi}^2) \tag{2-17}$$

and we look for solutions by taking the functional derivative of both sides with respect to $\tilde{\theta}$ and $\tilde{\phi}$ individually. If there are solutions with negative eigenvalues $\lambda_\theta$ or $\lambda_\phi$, then the static sG kink can lower its energy by deforming via these modes, and is therefore unstable. But we should stress that a solution of equation (2-15) with amplitude increasing with time is a better indication of a structural instability, since it shows that the deformation is dynamically possible.

Taking the functional derivatives of (2-17) leads to the eigenvalue problems

$$-\tilde{\phi}_{xx} + (1 - 2\,\mathrm{sech}^2 x)\tilde{\phi} = \lambda_\phi \tilde{\phi} \tag{2-18a}$$

$$-\tilde{\theta}_{xx} + (1 + 1/b - 6\,\mathrm{sech}^2 x)\tilde{\theta} = \lambda_\theta \tilde{\theta} \quad . \tag{2-18b}$$

These are both familiar Schrödinger problems with similar potentials, and

the spectrum for each is well known (Landau and Lifshitz 1958). The normalized bound and continuum states for each are

$$\tilde{\phi}_1 = (1/2)^{1/2} \text{ sech } x \quad ; \qquad \lambda_{\phi_1} = 0 \tag{2-19a}$$

$$\tilde{\phi}_k = (2\pi(k^2+1))^{-1/2}(\tanh x - ik)e^{ikx} \quad ; \quad \lambda_{\phi_k} = k^2 + 1 \tag{2-19b}$$

$$\tilde{\theta}_1 = (3/4)^{1/2} \text{ sech}^2 x \quad ; \qquad \lambda_{\theta_1} = 1/b - 3 \tag{2-20a}$$

$$\tilde{\theta}_2 = (3/2)^{1/2} \text{ sech } x \tanh x \quad ; \qquad \lambda_{\theta_2} = 1/b \tag{2-20b}$$

$$\tilde{\theta}_k = 3(2\pi(k^2+1)(k^2+4))^{-1/2}(\tanh^2 x - ik \tanh x - (k^2+1)/3)e^{ikx} \quad ;$$

$$\lambda_{\theta_k} = k^2 + 1 + 1/b \tag{2-20c}$$

The single bound state associated with $\tilde{\phi}$ has a zero eigenvalue and therefore involves no structural instability, but only reflects the continuous translational symmetry, namely that the kink can shift its position with no cost in energy. The first bound state associated with $\tilde{\theta}$, however, has a negative eigenvalue when $b > \frac{1}{3}$, and therefore indicates the possibility of a structural instability. This is the instability found by Kumar (1982) and Magyari and Thomas (1982), which, stated otherwise, occurs for $g\mu_B B_x > \frac{2}{3}AS$. This instability field is ~ 18 kG for $CsNiF_3$, and ~ 13.6 kG for CHAB. We cannot expect the sG kink to be a good solution for the original Hamiltonian (2-1) for $b > \frac{1}{3}$, since the static soliton is unstable, and the moving solitons are expected to be more unstable because of their larger out-of-plane tipping. This leads to the basic questions:

what is the nature of these excitations (the $2\pi$ rotations) beyond the sG stability limit, and for what parameter range is sG really valid? These questions have first been approached by others via variational Ansatz calculations, which we describe next.

Before going to these Ansatz calculations, a comment on the stability equations (2-15). One possible way to go about solving them is to assume $e^{i\omega t}$ time dependence, and expand the unknown solution in terms of the spectrum of (2-18). Then equations are obtained for the unknown expansion coefficients, and we still have an eigenvalue problem since the frequency $\omega$ is unknown. This approach seems to be a good one in principle, but has not yet produced a solution.

## 2.5 Various Ansatz Approaches

The exact static sG kink can be written as

$$\sin \frac{1}{2}\phi_{sG} = \operatorname{sech}[b^{1/2}\xi] \tag{2-21a}$$

$$\theta_{sG} = 0 \quad . \tag{2-21b}$$

But the stability analysis suggests that the distorted kink might be approximated by the Ansatz (Kumar 1982)

$$\sin \frac{1}{2}\phi = \operatorname{sech}(\xi/w) \tag{2-22a}$$

$$\sin \frac{1}{2}\theta = D \operatorname{sech}^2(\xi/w) \tag{2-22b}$$

D is a parameter measuring the amplitude of the deviation from the sG kink, and w is a width parameter. Both D and w are determined by extremizing the Lagrangian for the system with respect to variations in D and w. The Lagrangian L is obtained from H by the addition of what we call the "kinetic" term $K[\vec{S}]$,

$$K[\vec{S}] = \int dz\ S^z \frac{d}{dt} \tan^{-1}\left(\frac{S^y}{S^x}\right) \tag{2-23a}$$

or

$$K[\theta,\phi] = \varepsilon_0 \int d\xi\ \phi_\tau \sin\theta \quad , \tag{2-23b}$$

such that

$$L = K - H \tag{2-24}$$

If we assume Ansatz (2-22) is generally applicable for a moving distorted kink, then we change $\xi \to \xi - u\tau$ in (2-22), and after evaluating some integrals, the functionals K and H are found to be

$$K = -2\pi u D\left(1 - \frac{5}{16}D^2\right)\varepsilon_0 + O(D^5) \tag{2-25a}$$

$$H = 4\varepsilon_0\left[\frac{1}{w}F_1(D) + bwF_2(D)\right] \tag{2-25b}$$

where

$$F_1(D) = 1 + 2\left[2 - (1/D+1)^{1/2} \tanh^{-1}(1/D+1)^{-1/2} - (1/D-1)^{1/2}\tan^{-1}(1/D-1)^{-1/2}\right] - 2D^2\left(\frac{16}{15} - \frac{256}{315}D^2\right) \quad , \tag{2-25c}$$

$$F_2(D) = 1 + \frac{2}{3b} - \frac{2}{5}D^2 - \frac{16}{35b}D^4 \quad . \tag{2-25d}$$

K has been evaluated approximately, while H is exact. Extremizing L first with respect to w leads to

$$w = [F_1(D)/bF_2(D)]^{1/2} \tag{2-26a}$$

$$H = 8\varepsilon_0[bF_1(D)F_2(D)]^{1/2} \quad . \tag{2-26b}$$

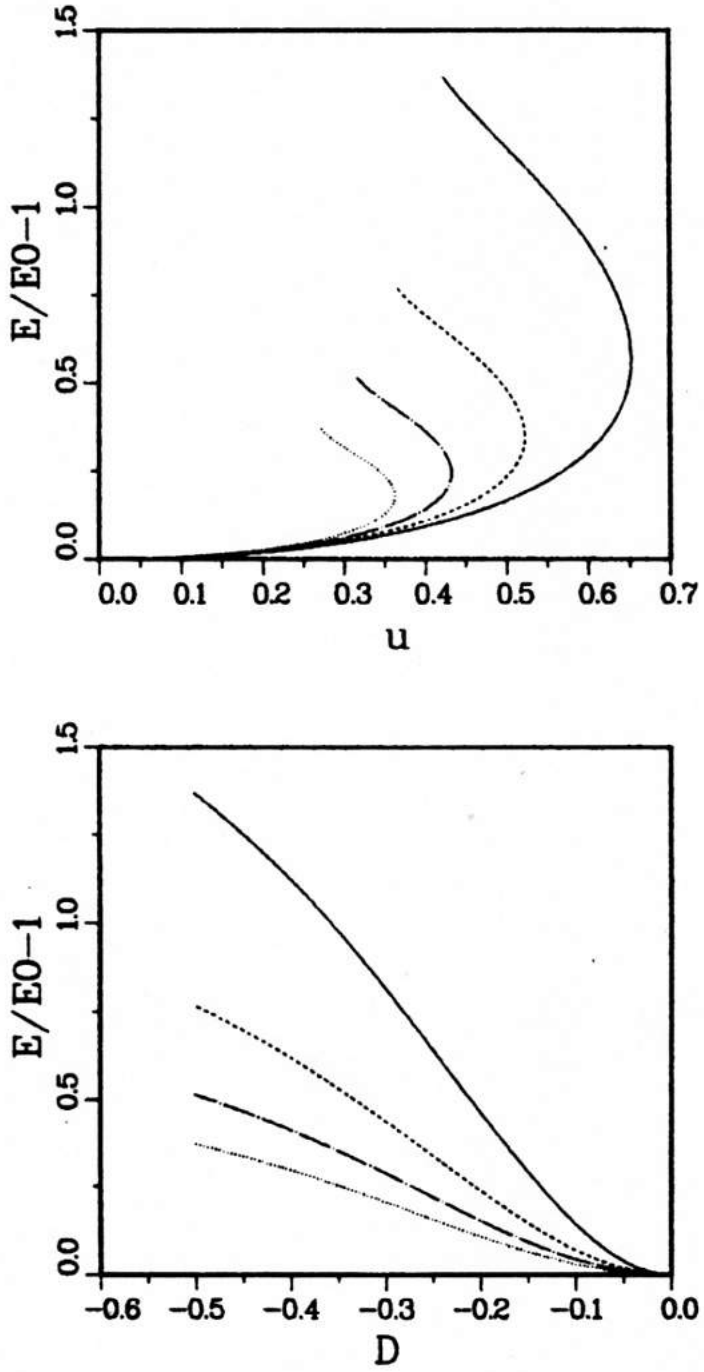


Figure 2.1a Kink energy vs. velocity u and vs. variational parameter D for Kumar's $\mathrm{sech}^2(\xi/w)$ Ansatz, at fields b = 0.02 (solid), b = 0.04 (dashed), b = 0.06 (chained) and b = 0.08 (dotted). The energy is normalized to the static sG kink energy.

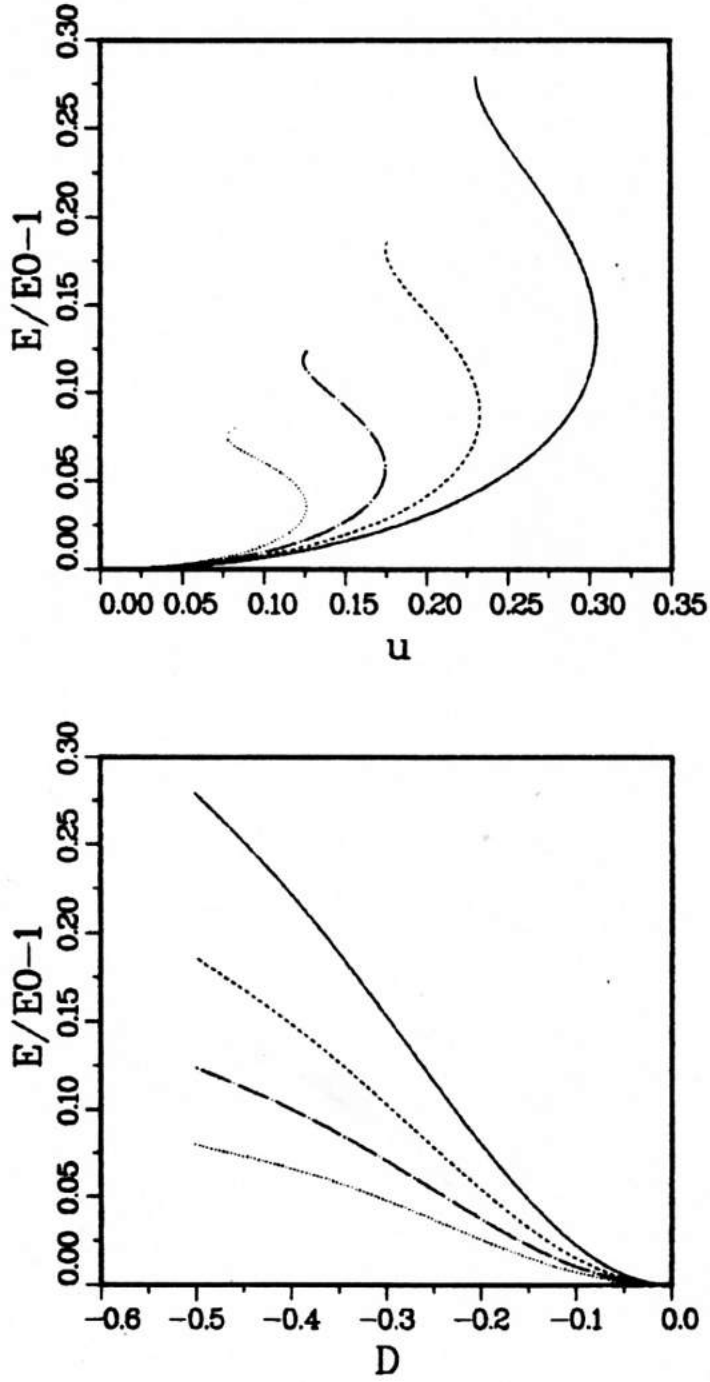


Figure 2.1b Results from Kumar's Ansatz, at fields b = 0.10 (solid), b = 0.13 (dashed), b = 0.16 (chained) and b = 0.19 (dotted).

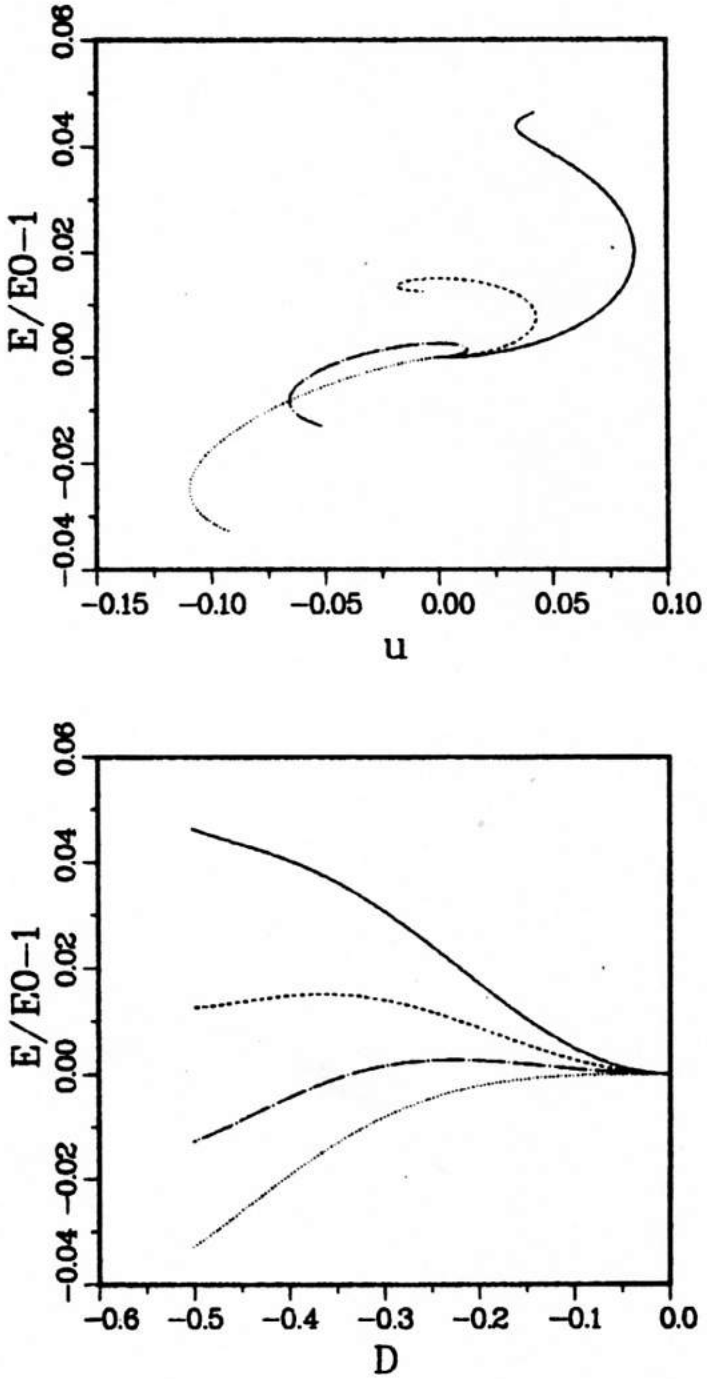


Figure 2.1c Results from Kumar's Ansatz, at fields b = 0.22 (solid), b = 0.26 (dashed), b = 0.30 (chained) and b = 0.34 (dotted).

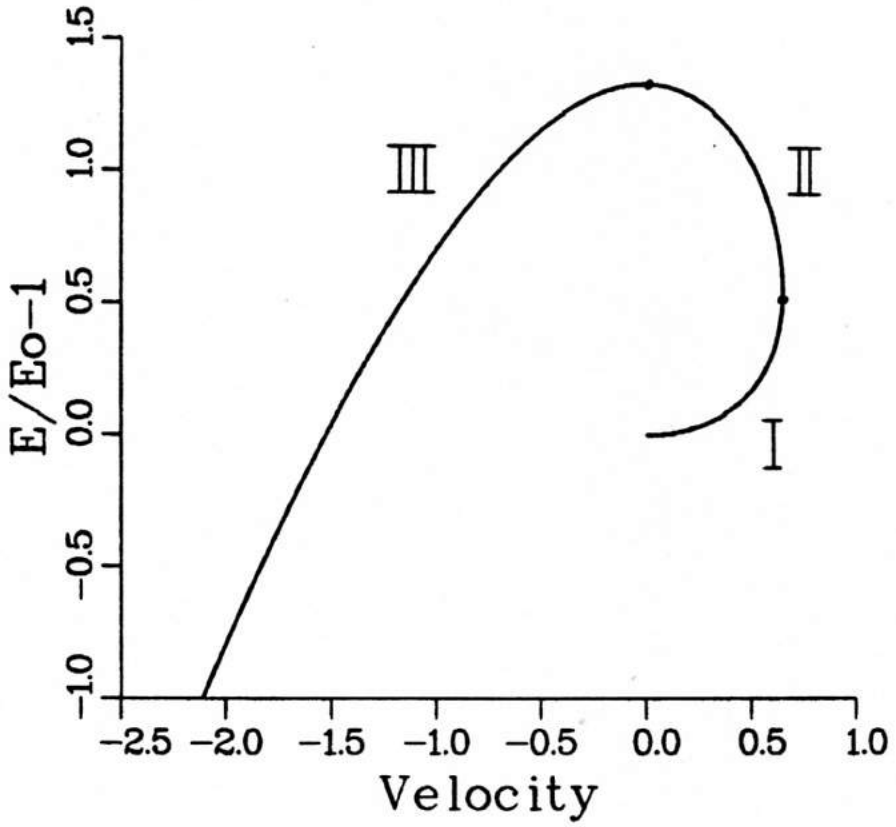


Figure 2.1d A dispersion curve derived from the Liebmann et al. Ansatz, for b = 0.03, used to illustrate the notation for the branches. Branch I is the low velocity, low energy limit, with positive effective mass and velocity. Branch II is the positive velocity, negative effective mass segment. Branch III is the negative velocity, negative effective mass segment. Stable kinks exist on all three branches. For $b > \frac{1}{3}$, only branch III exists.

Then extremizing with respect to D gives the velocity u as a function of D,

$$u = - \frac{\partial H/\partial D}{2\pi\varepsilon_0\left(1-\frac{5}{16}D^2\right)} \quad . \tag{2-27}$$

The values of D for zero velocity kinks are then determined by the extrema of H. In Figure 2.1, the kink energy, equation 2-26b; is plotted vs. D vs. u, by eliminating D using equation 2-27, for a series of fields b. For fields below and near the critical field $b_c = \frac{1}{3}$, there are two kinks with zero velocity. It will be seen from the Liebmann et al. Ansatz and the numerical simulation that the Kumar Ansatz loses its validity for $D \gtrsim 0.5$; there are always two zero velocity kink solutions for $b < b_c$. One is the static sG soliton (D = 0) and the other is a strongly distorted texture ($D \neq 0$) which cannot be described by sG. This distorted static kink has been shown to be stable by numerical simulations (Wysin et al. 1982). At the critical field $b_c = \frac{1}{3}$, the two zero velocity kinks have merged together; for fields $b > \frac{1}{3}$, only one static kink exists, along with a branch of "backwards" propagating kinks. These are called "backwards" since they do not satisfy the sG relationship $\theta = \phi_\tau$, but instead a reversed sign relationship $\theta \sim -\phi_\tau$. They move in the opposite direction from what would be expected for a sG profile. Other similar Ansätze have been made; see Kumar (1982a) and Magyari and Thomas (1982). These give similar results, with slightly different dispersion relations H(u). Originally the calculations were applied only to static kinks, but Liebmann et al. (1983) showed that the entire dispersion relation was obtained by extremizing the Lagrangian (which they called an "energy functional") instead of the Hamiltonian. They made a geometrically motivated Ansatz in terms of xyz spin components, in which the kink is

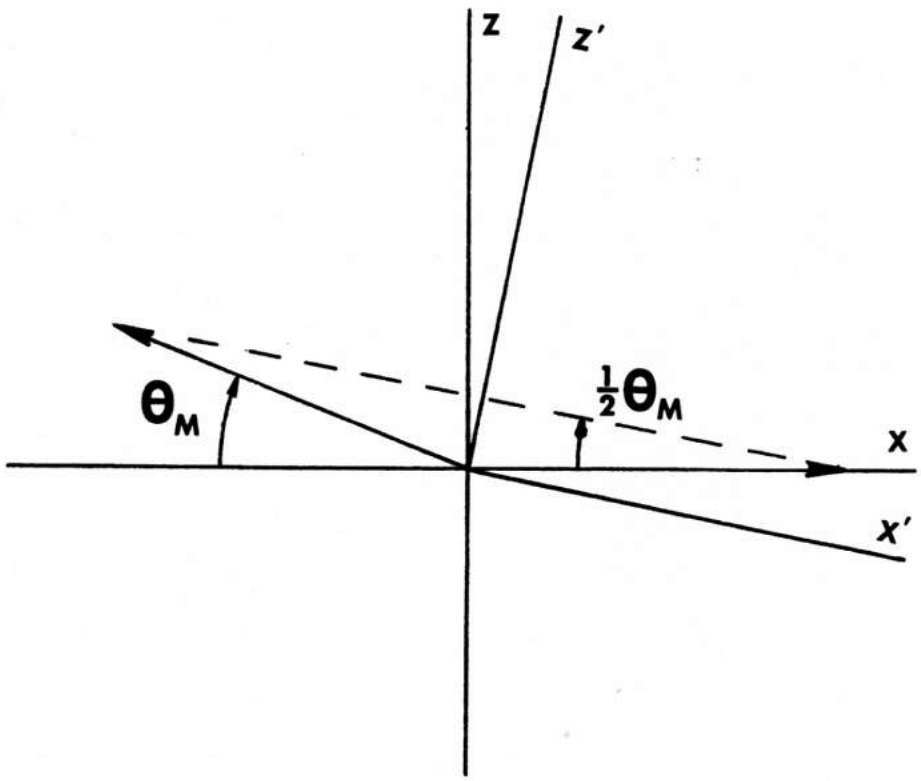


Figure 2.2 Geometry for the Liebmann et al. Ansatz. The arrow on the +x axis represents the spins at $z = \pm \infty$, the arrow at angle $\theta_m$ from the -x axis represents the spin at $z = 0$, the center of the kink. The dashed line represents the plane in which the tips of the spin vectors move.

described by a trajectory of the tips of the spin vectors on the unit sphere, along with the distribution of the spins along the trajectory. We describe this Ansatz here, since its theme will be applied later to the antiferromagnet.

## 2.6 The Liebmann et al. Ansatz

The Ansatz is formulated for unit spin vectors $\hat{\sigma}$. A trajectory is assumed which is the intersection of the unit sphere with a plane passing through the ground state point (1,0,0), and tilted at some angle $\frac{1}{2}\theta_m$ (see Figure 2.2). At the center of the kink, the spin is tilted up at an angle $\theta_m$ out of the easy plane. Then we have

$$\hat{\sigma}(\xi = -\infty) = (1,0,0)$$

$$\hat{\sigma}(\xi = 0) = (-\cos\theta_m, 0, \sin\theta_m)$$

$$\hat{\sigma}(\xi = +\infty) = (1,0,0) \quad . \tag{2-27}$$

In a primed coordinate system, tilted at an angle $\frac{1}{2}\theta_m$, the trajectory is a circle of radius $\cos\frac{1}{2}\theta_m$, so we write

$$\sigma^{x'} = \cos\tfrac{1}{2}\theta_m \cos\phi_L$$

$$\sigma^{y'} = \cos\tfrac{1}{2}\theta_m \sin\phi_L$$

$$\sigma^{z'} = \sin\tfrac{1}{2}\theta_m \quad , \tag{2-28}$$

where $\phi_L(\xi)$ describes the distribution of the spins on the trajectory. Transforming back to the unprimed frame,

$$\sigma^x = c^2 \cos\phi_L + s^2$$

$$\sigma^y = c \sin\phi_L$$

$$\sigma^z = cs(1 - \cos\phi_L) \quad , \tag{2-29}$$

where $c \equiv \cos \frac{1}{2}\theta_m$ and $s \equiv \sin \frac{1}{2}\theta_m$. (The transformation is

$$\sigma^x = c\sigma^{x'} + s\sigma^{z'}$$

$$\sigma^y = \sigma^{y'}$$

$$\sigma^z = -s\sigma^{x'} + c\sigma^{z'} \quad ).$$

Now an assumption must be made about the distribution of the spins on the trajectory, by specifying $\phi_L$. A sine-Gordon function is assumed,

$$\phi_L = 4\tan^{-1} \exp[(\xi - u\tau)/w] \quad . \tag{2-30}$$

Equations (2-29) and (2-30) define the Ansatz, with its variational parameters tilt $\theta_m$ and width w.

Evaluation of H for this Ansatz is straightforward. Evaluation of K requires more work; a step function at $\theta_m = 90°$ results. Liebmann et al. removed it on the grounds that is unphysical. Doing so, the Lagrangian is

$$L = - 2\pi us - 4c^2[1/w + (b + \frac{2}{3} s^2)w] \quad . \tag{2-31}$$

The rest of the calculation is the same as for the Kumar Ansatz, giving the energy E and velocity as functions of $\theta_m$

$$w(\theta_m) = (b + \tfrac{2}{3}s^2)^{-1/2} \tag{2-32a}$$

$$E(\theta_m) = 8\varepsilon_0 c^2/w \tag{2-32b}$$

$$u(\theta_m) = (8s/\pi w)(1 - \tfrac{1}{3}c^2w^2) \quad . \tag{2-32c}$$

It is possible to show that the functional K is related to the canonical momentum operator P for this system (Tjon and Wright 1977),

$$P = \int d\xi \, \sin\theta \, \frac{\partial \phi}{\partial \xi} \quad ; \quad \phi = \tan^{-1}(S^y/S^x) \quad , \tag{2-33a}$$

so that

$$K = -uP \quad . \tag{2-33b}$$

Then here we have the simple result

$$P = 2\pi s \quad . \tag{2-34}$$

As a result of this, the energy-momentum relationship is

$$E(P) = 8\varepsilon_0 (b + P^2/6\pi^2)^{1/2} (1 - P^2/4\pi^2) \quad . \tag{2-35}$$

A way to check this Ansatz against numerical simulations is to compute the energy of the distorted static kink. For a zero velocity kink, we need s = 0 (the sG limit) or

$$s^2 = s_m^2 = \frac{1}{3} - b \quad .$$

The width and energy are then

$$w_m = \left(\frac{1}{3}b + \frac{2}{9}\right)^{-1/2} \tag{2-37a}$$

$$E_m = 8\varepsilon_0 \left(\frac{1}{3}b + \frac{2}{9}\right)^{1/2} \left(b + \frac{2}{3}\right) \quad . \tag{2-37b}$$

m subscripts refer to this second static kink. Equation (2-36) has no solution for $b > \frac{1}{3}$; this second static kink exists only below the critical field. These expressions will be compared with data obtained numerically in the next section.

In the vicinity of this second static kink, the dispersion relation is an inverted parabola. We can define an effective mass $m^*$ by writing $E = E_m + \frac{1}{2}m^*u^2$, for $u \ll 1$, near this static kink. It is easy to show that this effective mass is given by $m^* = \frac{\partial^2 E}{\partial s^2} \cdot \left.\frac{\partial u}{\partial s}\right|^{-2}_{s_m}$. Similarly, an effective mass $m_0$ for the sG limit kink can be defined, near $s = 0$. From the Liebmann et al. Ansatz, these masses are found to be

$$m_0 = \frac{1}{4}\pi^2 b^{1/2}(\tfrac{1}{3} - b)^{-1}\varepsilon_0 \quad \text{for } b < \tfrac{1}{3} \text{ only} \tag{2-38a}$$

$$m^* = -\frac{\pi^2}{8}(\tfrac{1}{3}b + \tfrac{2}{9})^{\frac{1}{2}}(\tfrac{1}{3} - b)^{-1}\varepsilon_0 \quad \text{for } b < \tfrac{1}{3} \tag{2-38b}$$

$$m^* = -\frac{1}{4}\pi^2 b^{1/2}(b - \tfrac{1}{3})^{-1}\varepsilon_0 \quad \text{for } b > \tfrac{1}{3} \quad . \tag{2-38c}$$

We see that the second static kink has a negative effective mass, while the sG limit kink mass is always positive. Later on we will find it useful to refer to the positive mass sG limit kinks are belonging to "branch I", and the negative mass distorted kinks as belonging to "branch II" or "branch III", depending on whether $u > 0$ or $u < 0$.

An interesting point from these Ansatz calculations is that $E(u)$ can be a double-valued function. Once $\theta_m$ is specified, $E$ and $u$ are determined, but if the energy or velocity is specified, then there can be two solutions for $\theta_m$. This is obvious in Figure 2.3, where $E(u)$ for the Liebmann et al. Ansatz is plotted for various values of $b$. On these curves, $\theta_m$ varies from zero to $\pi$. Zero corresponds to a static sG kink, while near $\pi$ the Ansatz represents a small amplitude wave packet (a pulse). At $\theta_m = \pi$, the Ansatz has degenerated back to the ground state, and therefore zero energy (but not zero velocity).

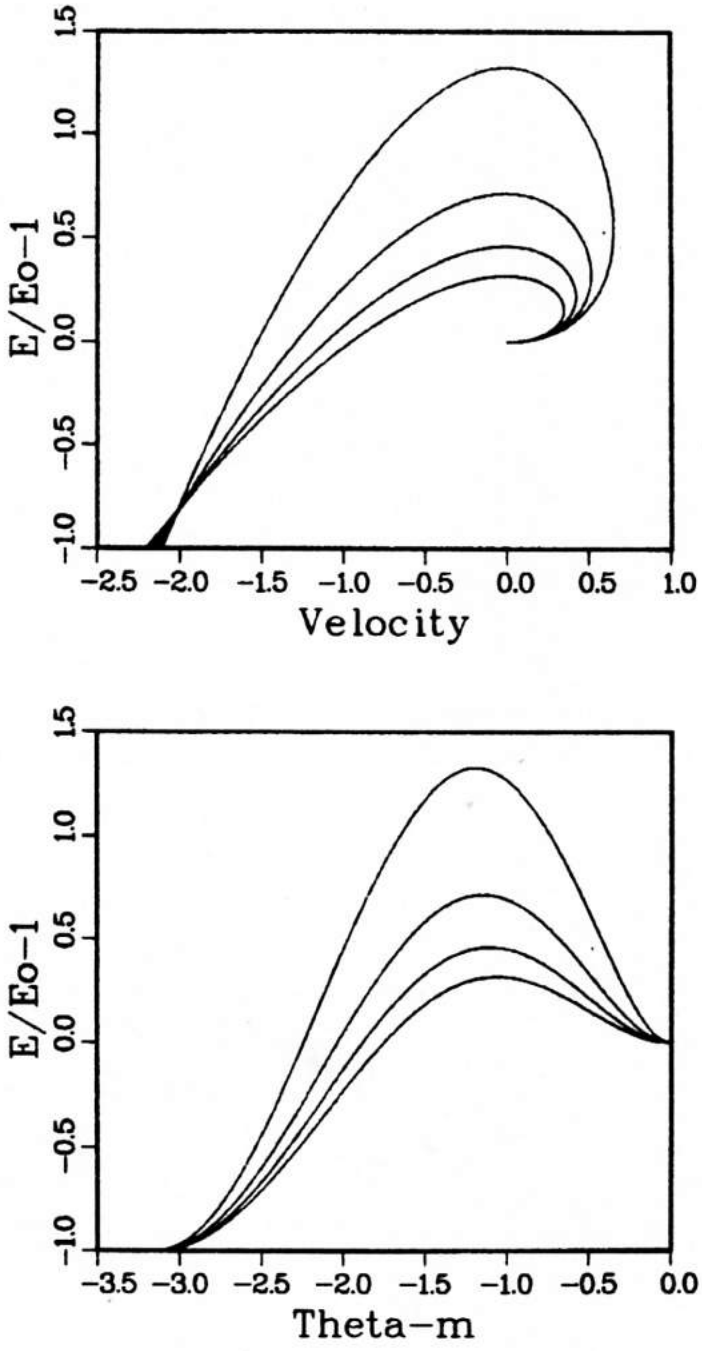


Figure 2.3a Kink energy vs. velocity u and vs. variational parameter $\theta_m$ for the Liebmann et al. Ansatz, at fields b = 0.02, 0.04, 0.06 and 0.08, from top to bottom. The energy is normalized to the static sG kink energy.

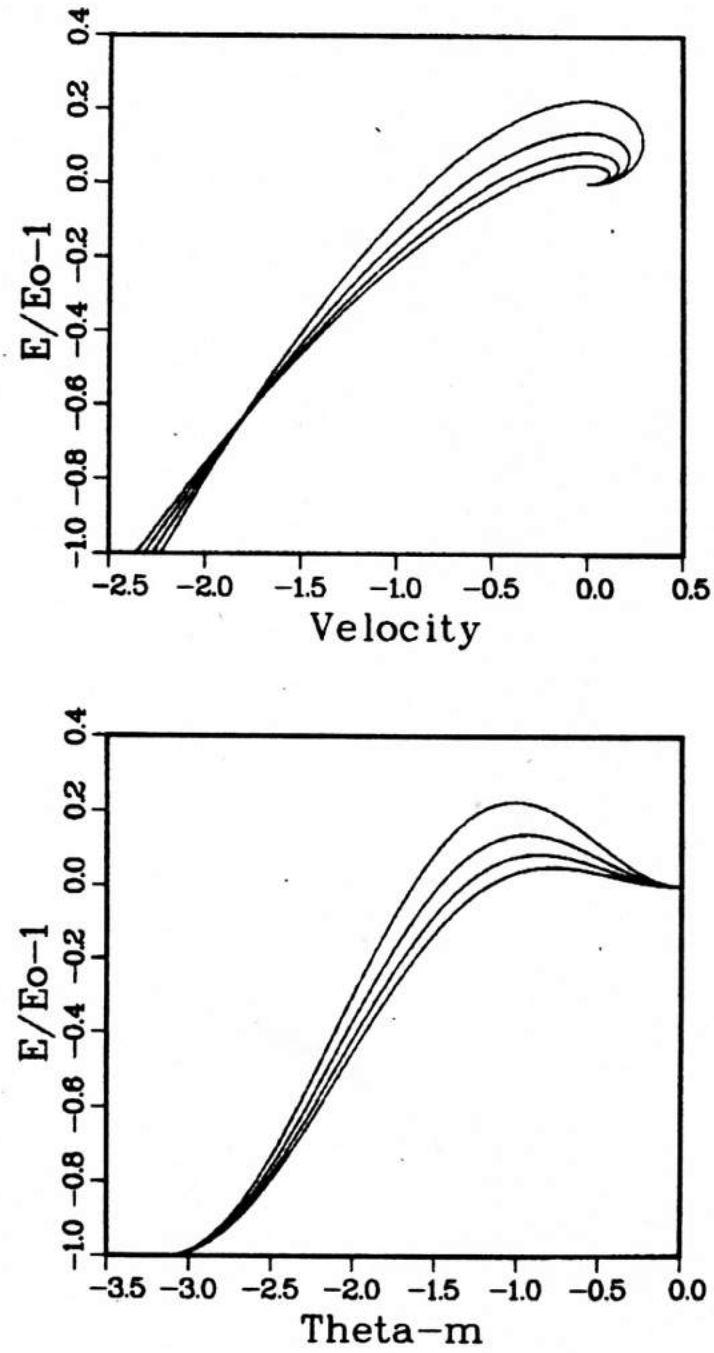


Figure 2.3b Results from the Liebmann et al. Ansatz, at fields b = 0.10, 0.13, 0.16 and 0.19, from top to bottom.

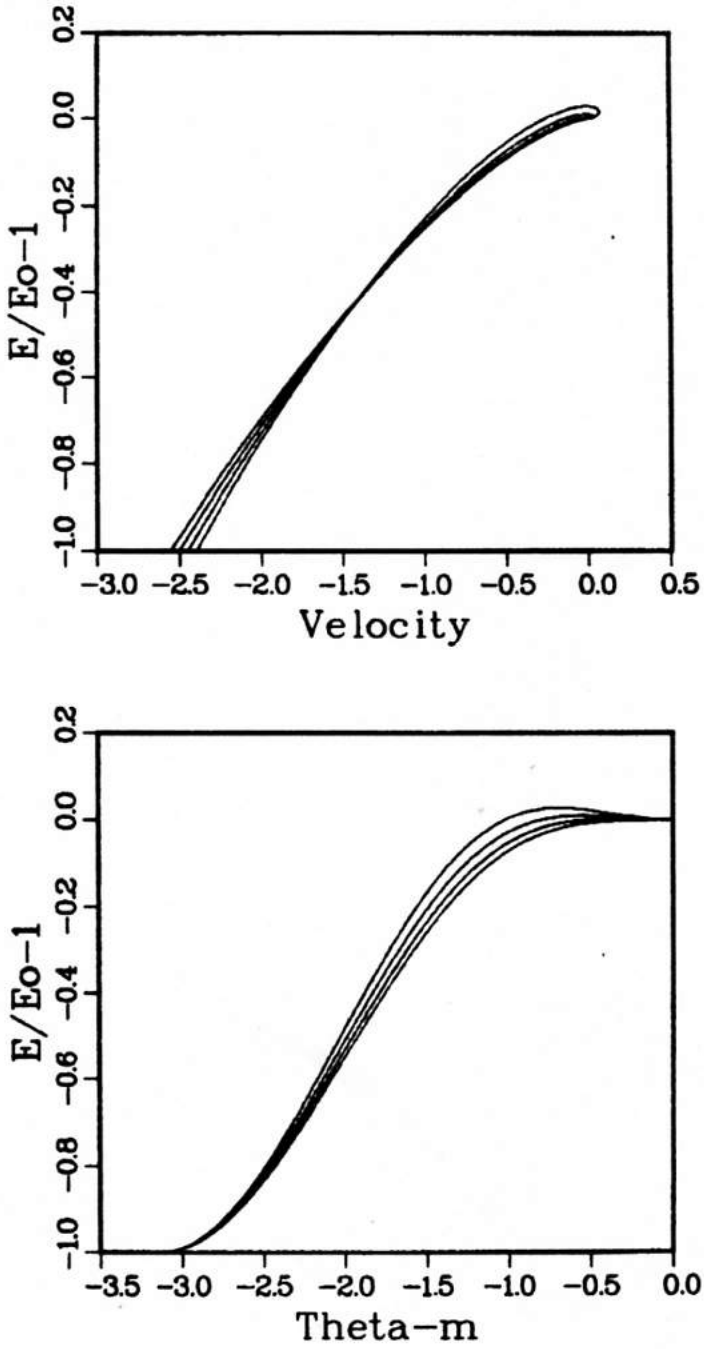


Figure 2.3c Results from the Liebmann et al. Ansatz, at fields b = 0.22, 0.26, 0.30 and 0.34, from top to bottom.

The advantage of this type of Ansatz is threefold: 1) it is motivated by geometrical intuition, using restrictions of the boundary conditions; 2) it explicitly allows for large out-of-plane motions which are excluded from the sine-Gordon limit, but certainly implied by the stability analysis; 3) it avoids complications which arise near $\theta = \frac{1}{2}\pi$ in spherical polar coordinates for the other Ansätze. These points seem to be responsible for its success and agreement with earlier numerical simulations (Wysin et al. 1982).

## 2.7 Numerical Simulation of Magnetic Kinks

The discrete equations of motion (2-5) were integrated numerically on a lattice ranging from 100 to 180 spins. The system size was adjusted to accommodate the wider kinks at low fields (recall kink width $\sim \beta^{-1/2}a$). Periodic boundary conditions were used in all cases. A variable time step, variable order Adams-Pece predictor corrector integration scheme was used (Shampine and Gordon 1975) to solve the coupled system of ordinary differential equations. We checked the accuracy of the method by noting that energy was conserved to better than 1 part in $10^5$ for our time intervals of integration. Most of this work was done using $\alpha = 2A/J = 0.0954$, in order to test the validity of continuum theories and minimize discreteness effects.

In a typical experiment, Equations (2-9) and (2-10) were used to specify the initial data, discretized on the lattice, as a sG kink of velocity $u_{sG}$. Then the subsequent time evolution was followed, expecially the kink position and velocity. We defined the position of the kink as the point at which the in-plane angle $\phi$ is $\pi$, interpolated between the lattice points. Although this definition can lead to a rapidly fluctuating velocity component if there are asymmetric shape oscillations, all

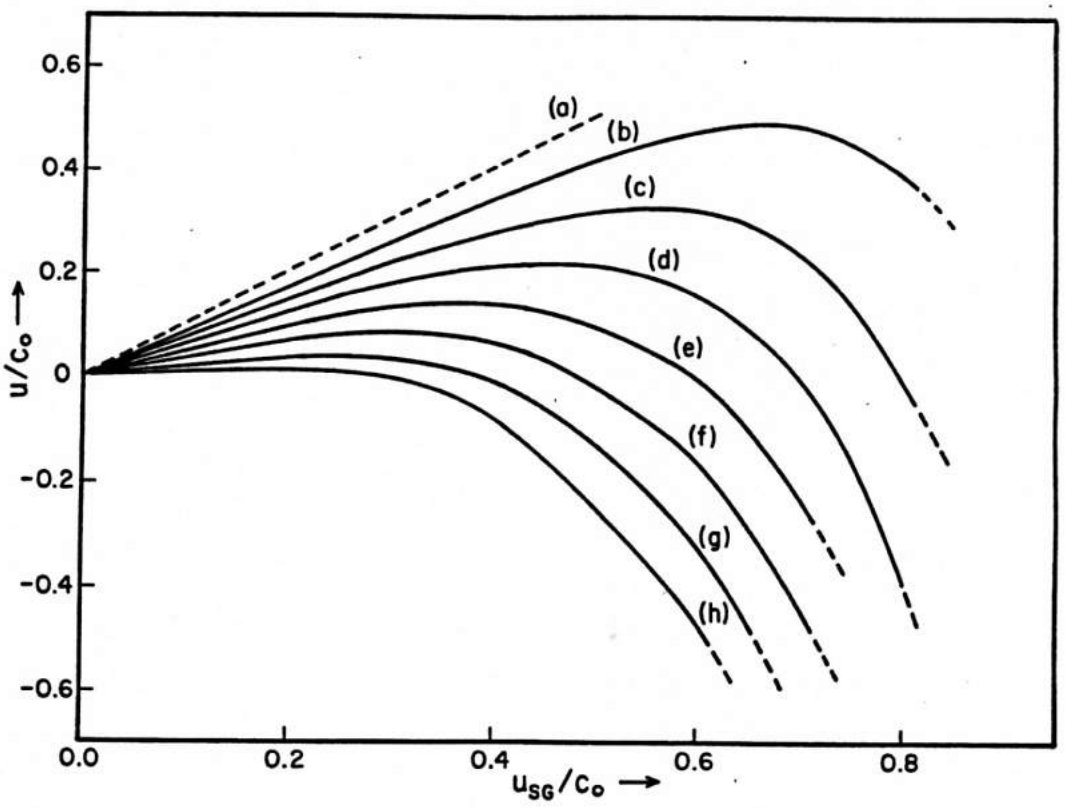


Figure 2.4 Results from the numerical simulation. The actual average kink velocity $\bar{u}$ is plotted vs. the velocity $u_{sG}$ of the sG kink initial condition, for $\alpha = 0.0954$ and fields b = (a) $0^+$ (i.e. sG limit), (b) 0.0419, (c) 0.0239, (d) 0.1258, (e) 0.1677, (f) 0.2096, (g) 0.2516 and (h) 0.2935.

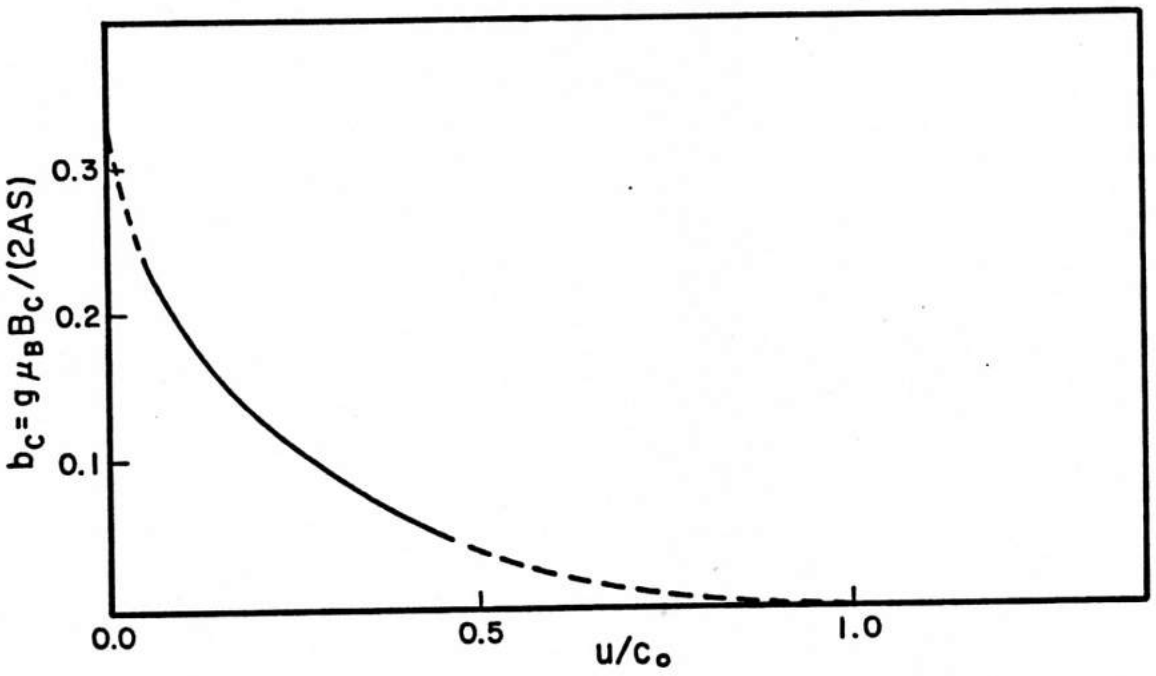


Figure 2.5 The maximum kink velocity $\bar{u}_{max}$ vs. applied magnetic field b, as derived from Figure 2.4.

results have been plotted in terms of the average kink velocity u in order to remove this effect. Usually the initial conditions did not correspond to an exact traveling wave, so that oscillations were unavoidable without special methods. Initially we did not use any special techniques, but simply measured the average actual velocity u as a function of the input sG velocity $u_{sG}$, varying the magnetic field as a parameter. These results are shown in Figure 2.4.

The behavior was found to be strongly unlike sine-Gordon even for fields $b < b_c$. (Except for the static sG limit $u_{sG} = 0$). Even for arbitrarily small nonzero velocities, u was found to be less than $u_{sG}$. As a function of $u_{sG}$, u first increases, then reaches a maximum value $u_{max}(b)$, and then begins to decrease, all while the energy continuously increases. The maximum velocity $u_{max}(b)$ decreases with increasing magnetic field (see Figure 2.5). For $b > b_c$, u is a decreasing function of $u_{sG}$. This is the regime where there are only backwards propagating kinks; the behavior is very strongly unlike sine-Gordon. The instability predicted analytically is not truly structural, but manifests itself through this non-sG behavior.

Especially for higher velocity kinks (larger $u_{sG}$), the above method could not give an accurate determination of the kink energy, since the insufficient initial conditions (not a true traveling wave) showed relaxation accompanied by the emission of spin waves. The presence of spin waves causes an overestimation of the kink energy since there is no simple way to separate the spin wave energy from the kink energy. All we can compute numerically is the total system energy. To correct this, we time averaged the xyz spin components of the kink in its own moving reference frame, and then used this time averaged profile as initial conditions. A typical averaging time interval was 200 ($\hbar$/JS) time units. After time

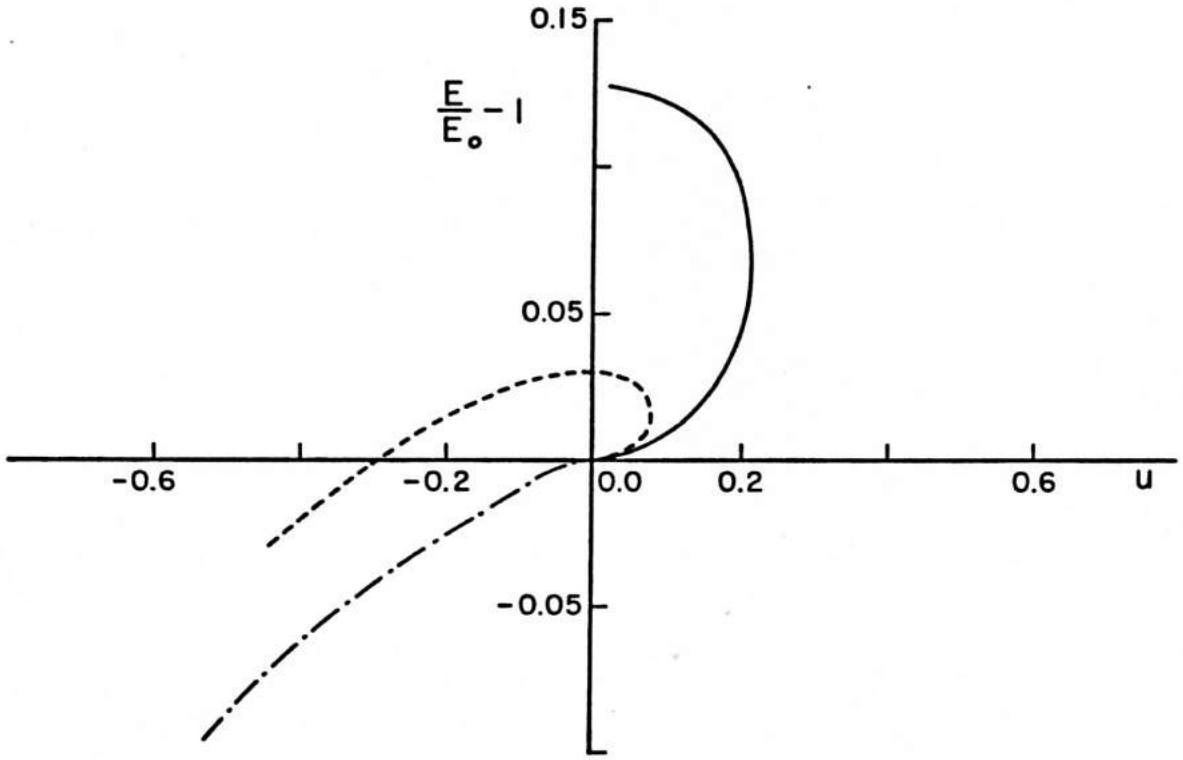


Figure 2.6 Kink energy dispersion as obtained by time averaging procedure, for $\alpha = 0.0954$, and fields b = 0.1258 (solid), b = 0.2096 (dashed), and b = 0.4193 (chained). The energy is normalized to the static sG energy.

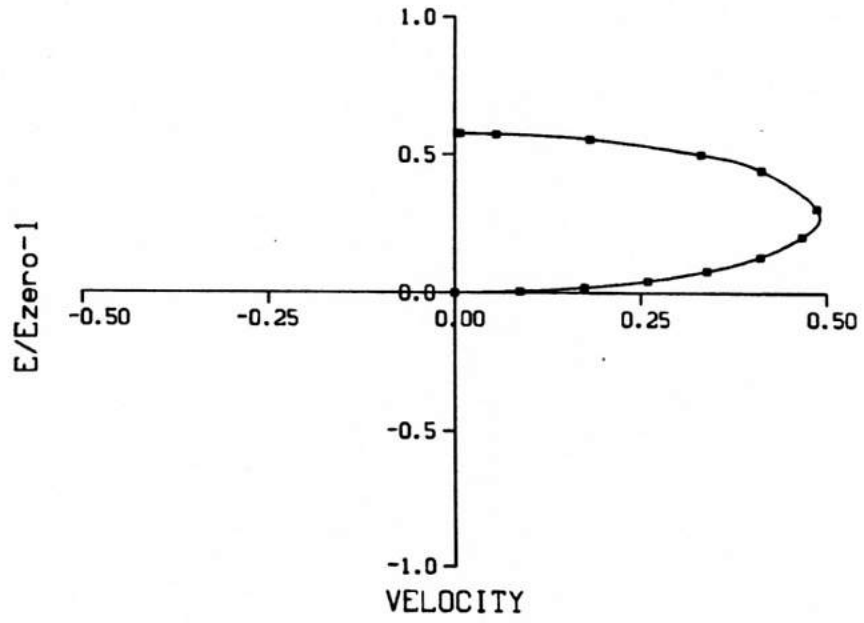


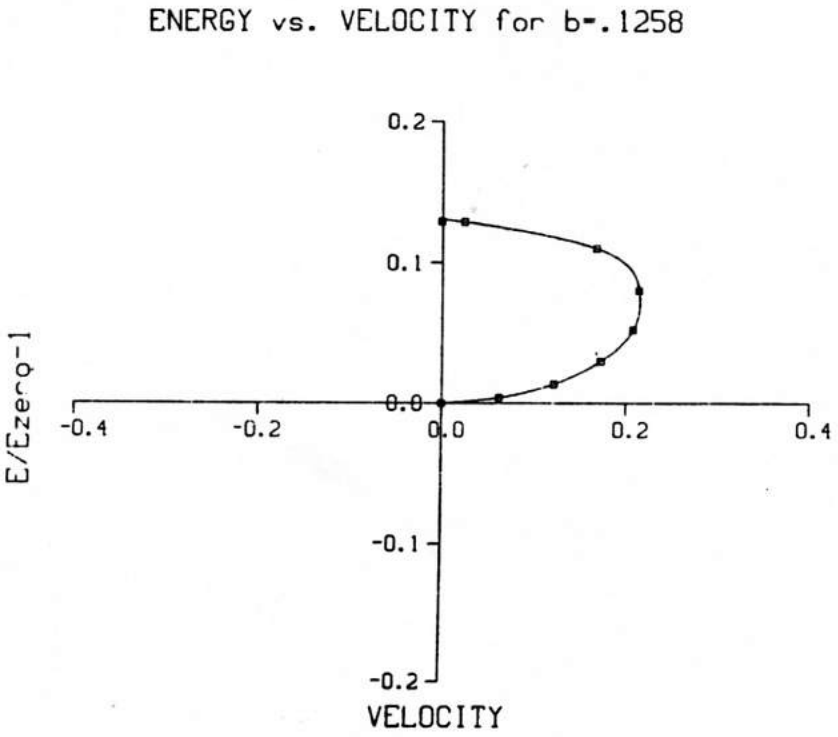


Figure 2.7a Further details of kink energy dispersion, from the numerical simulation, for $\alpha = 0.0954$ and $b = 0.04193$ and $b = 0.1258$. The points are from the simulation, the curves are spline fits.

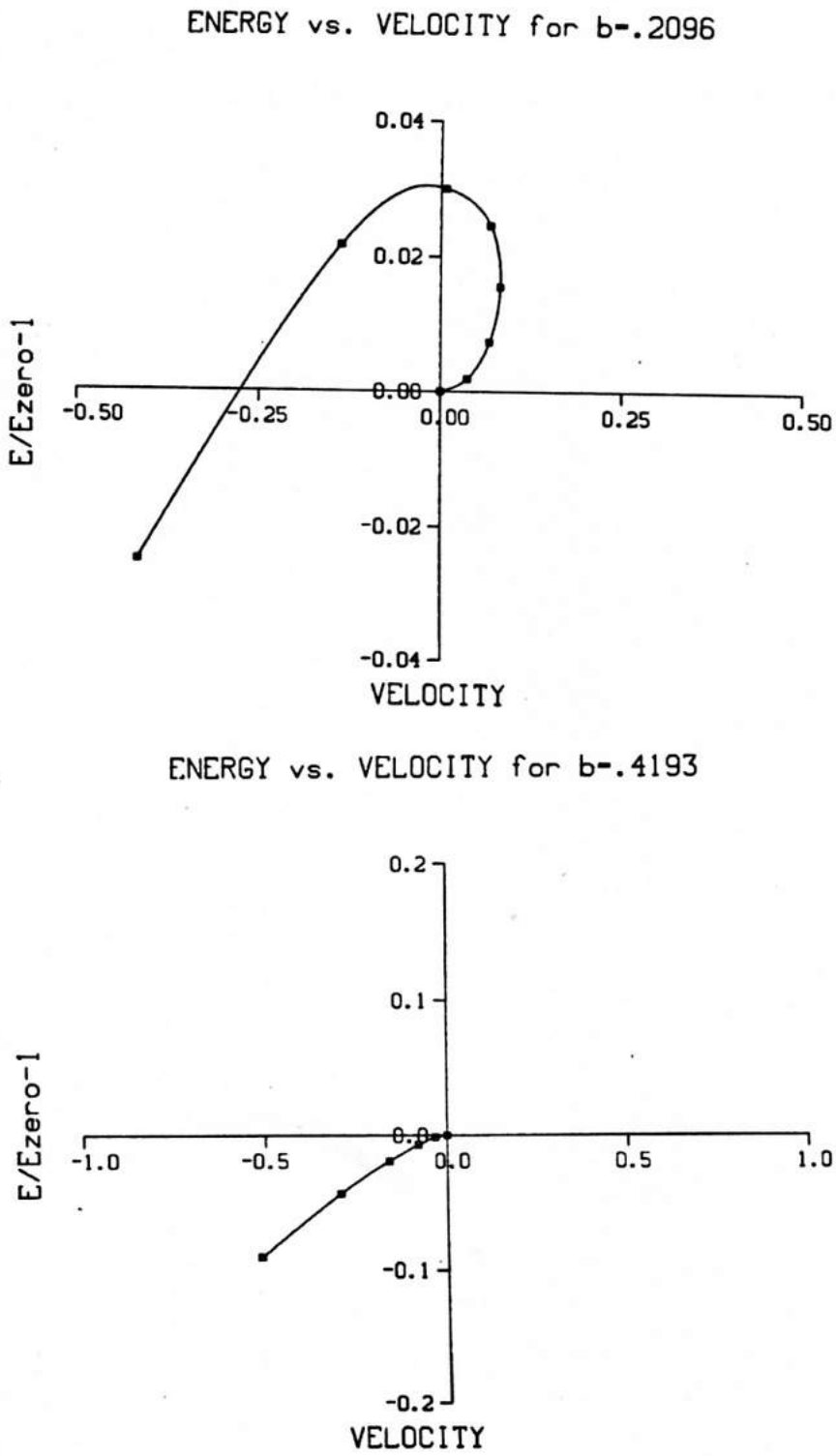


Figure 2.7b Further details of kink energy dispersion, from the numerical simulation, for $\alpha = 0.0954$ and $b = 0.2096$ and $b = 0.4193$. At $b = 0.4193$ only branch III exists.

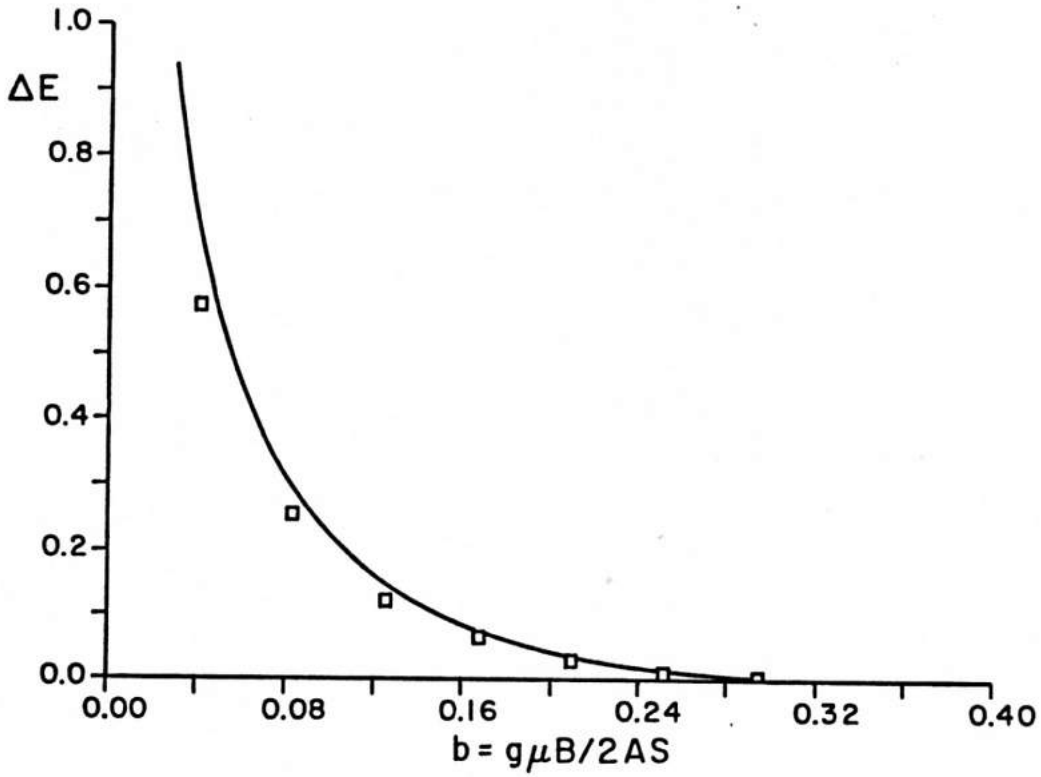


Figure 2.8 The energy of the second static kink (the maximum energy kink) vs. applied field b. Here $\Delta E \equiv E/E_0 - 1$. The solid curve is obtained from the Liebmann et al. Ansatz, equation 2-37b. The points are from the numerical simulation.

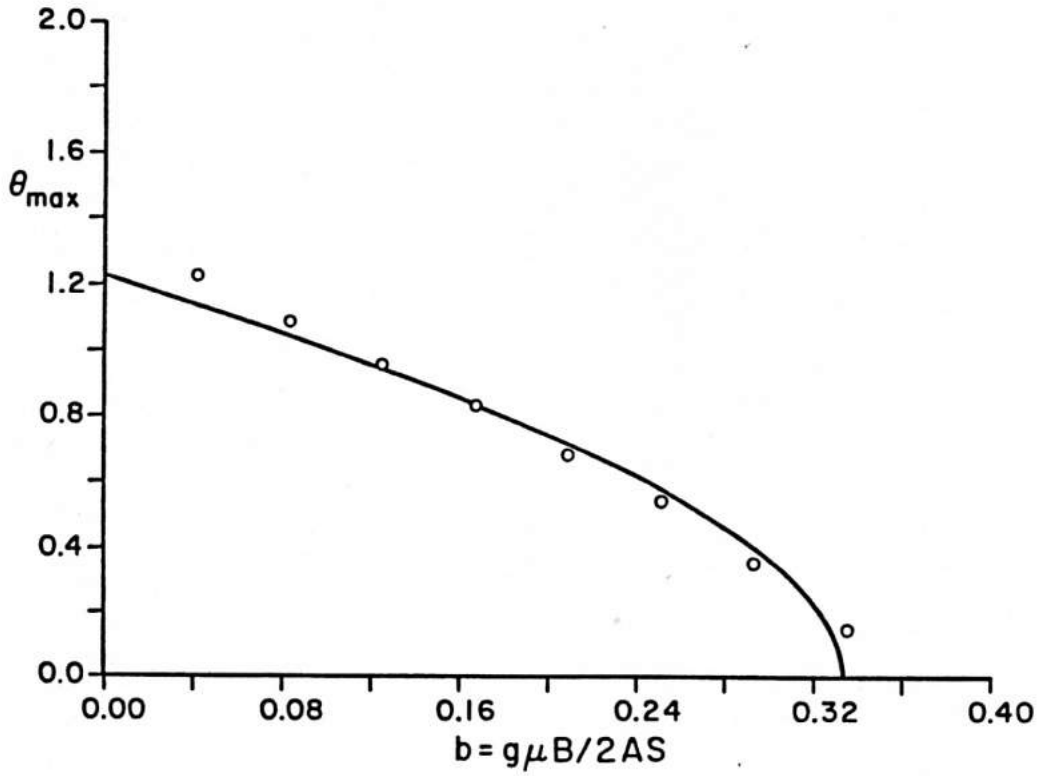


Figure 2.9 The maximum out-of-plane angle $\theta_{max}$ vs. applied field b for the second static kink. The solid curve is derived from the Liebmann et al. Ansatz, equation 2-36. The points are from the numerical simulation.

averaging twice, the resulting profile was usually an accurate traveling waveform, except in extreme cases of large $u_{sG}$ or narrow kink width. This profile was then used to initiate the simulation. Again u was measured as before. In Figures 2.6 and 2.7 the dispersion relation E(u) is plotted for a series of field values, for fixed $\alpha$.

The Liebmann et al. Ansatz results are consistent with these downward ments, which were the first evidence for structurally stable, strong non-sG behavior, even for low fields and velocities, although initially we did not used the time averaging procedure and therefore had overestimated the enrgy. To further compare our data and the Liebmann et al. Ansatz, we measured the energy $E_m$ and maximum out-of-plane angle $\theta_m$ for the distorted static kink (the maximum energy kink for $b < b_c$), as a function of b. These are plotted in Figure 2.8 and Figure 2.9 respectively. The full curves are derived from the Ansatz, and the data points are from the numerical simulation. The agreement is good in both cases. One should note that the Ansatz slightly overestimates the energy, as is expected.

Regions of the dispersion curves where the curvature is negative ($\partial^2 E/\partial u^2 < 0$) have previously been thought of as unstable (Magyari and Thomas 1982). These simulations demonstrated the stability of these negative mass regions, as well as the rest of the dispersion curve. There is no sudden change in the stability or profile of the kink at the maximum velocity point of the dispersion curves (i.e. the point connecting branch I to branch II). There is only a smoothly increasing out-of-plane tipping, and consequent deviation from the sG description, as one moves out from the origin along the dispersion curve. This is accompanied by the anisotropy becoming an increasing fraction of the total energy, while

the width and velocity decrease. This is inconsistent with the sG picture and can be understood only in terms of a distorted texture.

## 2.8 Discussion

The numerical simulations were stimulated by the possibility of a kink instability predicted analytically, and the hope that this would be easily verified numerically. The results of these simulations were somewhat unexpected, in that a static sG kink for $b > \frac{1}{3}$ did not spontaneously decay to a distorted texture. Also, the dispersion relations found were contrary to expectations, especially the existence of stable negative mass branches (II and III), and the existence of only a backward branch (III) for fields beyond the critical field $b_c = \frac{1}{3}$. Only the low energy, low velocity branch I kinks can be thought of as perturbed sG kinks. Generally the freedom of large out-of-plane motions profoundly affects the dynamics in such a way that the sG equation is not adequate to describe single kink dynamics. Even for $b \ll b_c$, the distorted texture exists and would be expected to affect the thermodynamics. For $b > b_c$, a thermodynamic description based on sG theory will be expected to be entirely inadequate, since the limiting sG branch does not even exist then. In order to further support these conclusions, kink-antikink collisions are studied next. A question to ask is: are these non-sG kinks stable during collisions, retaining their shape afterwards? And if not, then what is the result of a collision? These questions are answered in the next chapter.